Acta Neuropathol (1996) 92 : 75–89

REGULAR PAPER

Brian J. O'Neil · Sarah S. Alousi · Blaine C. White
José A. Rafols

Ultrastructural consequences of radical damage before and after differentiation of neuroblastoma B-104 cells

Received: 11 December 1995 / Revised, accepted: 26 February 1996

Abstract There is abundant evidence that the pathophysiology leading to neuronal death during post-ischemic brain reperfusion involves radical-mediated damage. Although the ultrastructural alterations accompanying brain ischemia and reperfusion are well characterized, little is known about the ultrastructural alterations that are specific to radical damage. This study examines in differentiated and undifferentiated neuroblastoma B-104 cells the viability (by dye exclusion) and ultrastructural consequences of radical damage initiated by 50 μ*M* cumene hydroperoxide (CumOOH). Differentiation was most notably associated with formation of neurites and an extensive cytoskeletal feltwork. CumOOH-induced cell death was increased after differentiation and was blocked by the iron chelator DETAPAC. The ultrastructural characteristics of radical damage here included: (1) plasmalemmal holes that appear to undergo "patching" by well-organized membrane whorls, (2) accumulation of numerous free ribosomes, (3) markedly increased vesicular trafficking about the Golgi accompanied by Golgi transformation from cisternal organization to clusters of vacuoles with numerous fusing vesicles, (4) development of large multi-layered vacuoles that include damage membranes and organelles and appear to undergo extrusion from the cell, and (5) a general loss of cytoplasmic volume. These ultrastructural alterations developed more rapidly and were consistently more advanced in differentiated cells throughout the 6-h time course. In differentiated cells radical damage also induced the disorganization and subsequent loss of the extensive feltwork of cytoskeletal elements. There was little damage to the membranes of the nuclear envelope and mitochondria. Our observations in this system are strikingly similar to ultrastructural alterations in Golgi and ribosomal organization seen in vulnerable neurons during post-ischemic brain reperfusion and suggest that these alterations during reperfusion reflect the consequence of radical-mediated damage.

Key words Radicals · Neuron · Ultrastructure · Differentiation · Golgi

B. J. O'Neil (✉)
Emergency Department, Detroit Receiving Hospital,
4201 St. Antoine, Detroit, MI 48201, USA
Fax: 1-313-993-7703

B. J. O'Neil · S. S. Alousi · B. C. White
Department of Emergency Medicine,
Wayne State University School of Medicine,
Detroit, MI 48201, USA

B. C. White
Department of Physiology,
Wayne State University School of Medicine,
Detroit, MI 48201, USA

J. A. Rafols
Department of Anatomy and Cell Biology,
Wayne State University School of Medicine,
Detroit, MI 48201, USA

Introduction

Ischemia and reperfusion cause damage to selectively vulnerable neurons (SVNs) in the brain by mechanisms that involve both ischemia-induced elevation of cytosolic calcium and oxygen radicals generated during reperfusion [29]. We have previously reported evidence that (1) thiobarbituric acid-reactive radical reaction products accrue during reperfusion in the SVNs of the cortex and hippocampus [30], (2) that in SVNs these reaction products appear most concentrated in the area where the Golgi apparatus is located, and (3) that the Golgi apparatus during reperfusion undergoes prominent morphological alterations including formation of grossly aberrant intracellular vesicles [19].

These findings suggest that reperfusion-induced radical damage is the initial cause for the observed formation of the aberrant intracellular vesicles. Ample previous evidence also shows that differentiation adversely affects cellular survival after radical-mediated damage [29]. In the present study we have examined neuronally differentiated and undifferentiated neuroblastoma B-104 (NB-104) cells to characterize the survival and ultrastructural consequences along a 6-h time course after a discrete insult with an or-

ganic alkoxyl radical (generated from 50 μ*M* cumene hydroperoxide, CumOOH).

Methods

Cell culture

Neuroblastoma line B-104 cells were utilized. This cell line was developed from chemically induced brain tumors in rats, becomes neuronally differentiated in the presence of dibutryl-cAMP and theophylline. After differentiation this cell line has neurotransmitter receptors and the ability to synthesize neurotransmitters [22], and can be grown in serum-free media [4]. The NB-104 cell line was maintained in a solution prepared by mixing: 2 parts fetal calf serum with 1.42 m*M* $NaHCO_3$, 300 m*M* HEPES, penicillin, streptomycin and gentamycin; 4 parts horse serum; 37 parts Ham's F12 medium (Gibco); and 37 parts the Dulbecco-Vogt modification of Eagle's medium (Gibco). Subculturing was performed when the cells grew to near confluence. Differentiation of NB-104 cells into neurons was stimulated by growing the cells in the presence of 1 m*M* dibutryl-cyclic AMP and 1 m*M* theophylline. Morphological evidence of neurite growth induce by differentiation [16] was obtained by in situ fixation with 2% glutaraldehyde, staining with crystal violet, and microscopic examination.

Radical damage to undifferentiated and differentiated cells

NB-104 cells were simultaneously subcultured for 72 h in media with and without 1 m*M* dibutryl cAMP and 1 m*M* theophylline. After this the growth media was removed, the cells were gently washed once in F-12 and then incubated at 37° C in fresh F-12, which contained 3 μ*M* $FeSO_4$. Radical damage was then initiated in the culture dishes in undifferentiated and differentiated cells by addition of CumOOH to a final concentration of 50 μ*M*, thus generating the cumene alkoxyl radical by the reaction:

$$Fe^{2+} + CumOOH \rightarrow Fe^{3+} + OH^- + CumO^\bullet$$

The generation of an organic alkoxyl radical initially outside the cell is a model for the scission of hydroperoxides by ferrous iron, which we have suggested is released extraneuronally during postischemic reperfusion [26]. Tissue damage by such radicals is thought to involve principally the exponential chain reactions of lipid peroxidation in membranes [2, 29]. DETAPAC (final concentration 1.0 m*M*) was included in concurrent control experiments to confirm the iron dependence of the damage. Reactions were stopped after 2, 4, and 6 h by adding DETAPAC to a final concentration of 1.0 m*M*. Our previous work with iron-dependent radical damage to DNA has shown that DETAPAC:iron ratios of greater than 16 : 1, such as we establish here, will terminate iron-dependent radical reactions [27]. Cell viability as assessed by trypan blue dye exclusion in triplicate samples obtained at selected points during the time course of radical damage; 500 cells were counted in each of the triplicate samples to establish the percentage of viable cells.

Preparation of cells for electron microscopy

Concomitant with the sampling for assessment of cell viability, cells exposed to radical damage in separate culture dishes were simultaneously aldehyde-fixed and agarose-embedded in situ. Lomelt agarose (3.0%) was prepared in 140 m*M* NaCl and 20 m*M* $NaHPO_4$ (pH 7.4); this was then cooled at 40° C, and glutaraldehyde and paraformaldehyde were added to final concentrations of 5.0% and 1.0% respectively. At the appropriate time this solution, in a volume equal to that of the media in the dish, was added into the culture dish and mixed by gentle swirling, after which the agarose was allowed to set. The agarose disks were then removed, placed between sheets of Whatman filter paper, and vacuum dried on a gel dryer without heat. The cells in the thin transparent disks were post-fixed with 0.5% OsO_4 for 2 h, washed repeatedly in phosphate buffer, dehydrated in graded alcohols, cleared with propylene oxide, and embedded in an Epon-Araldite mixture. Thin disks of polymerized resin containing the cells were examined under a light microscope and microdissected into small (2 mm^2) chips containing cell clusters; these chips were then attached to plastic chucks for ultrathin sectioning. Ultrathin sections were obtained with a diamond knife on a LKB ultramicrotome, collected on copper grids, stained with uranyl acetate and lead citrate, and examined with a JEOL-JEM 1010 electron microscope.

Results

Cell differentiation

The gross structural effects of differentiation in theophylline and dibutryl-cAMP were examined utilizing cresyl violet staining and light microscopy. The differentiation

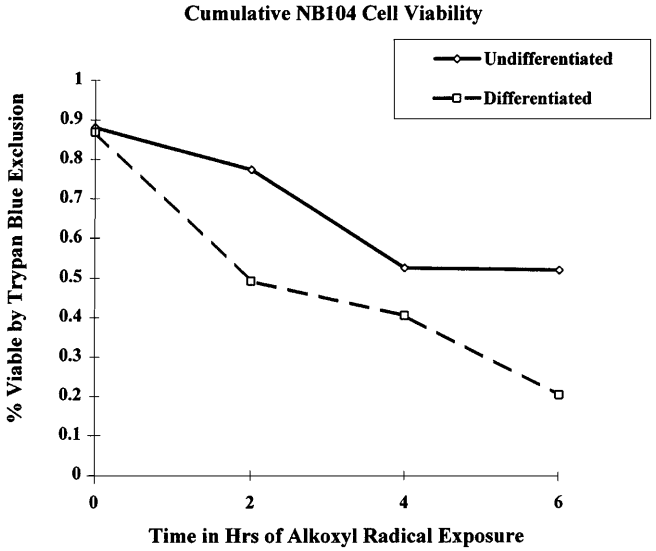

Fig. 1 Viability of differentiated and undifferentiated neuroblastoma B-104 (NB-104) cells following exposure to 50 μ*M* cumene hydroperoxide. Radical damage was initiated in differentiated and undifferentiated NB-104 cells by adding cumene hydroperoxide to a final concentration of 50 μ*M*. Radical reactions were stopped at different times during the 6-h time course by adding DETAPAC to a final concentration of 1 m*M*. Cell viability was assessed by trypan blue dye exclusion in triplicate 500-cell counts at selected points during the time course. There was no loss of cell viability if 1 m*M* DETAPAC was present in the medium prior to addition of cumene hydroperoxide (data not shown)

Fig. 2 A–C Electron micrographs of profiles of undifferentiated ▶ control NB-104 cells. **A** A portion of a dividing cell at metaphase. *Arrows* point at membranous 'whorly' bodies in the cytoplasm of the cell. **B** A portion of a nondividing cell. The nucleus *(nu)* contains multiple nucleoli and evenly dispersed heterochromatin. **C** Detail of the nucleus *(nu)* and cytoplasm of a nondividing cell. A thin rim of densely clumped chromatin granules lines the inner aspect of the nuclear envelope. A *small arrow* points at a nuclear pore in the envelope. The cytoplasm contains short, somewhat-dilated cisternae of rough endoplasmic reticulum (RER), ribosomal arrays and an array of smooth membranous tubules and sacs *(large arrow)*. *Bar* in **A** (also for **B**) = 1.0 μm, *Bar* in **C** = 1.0 μm

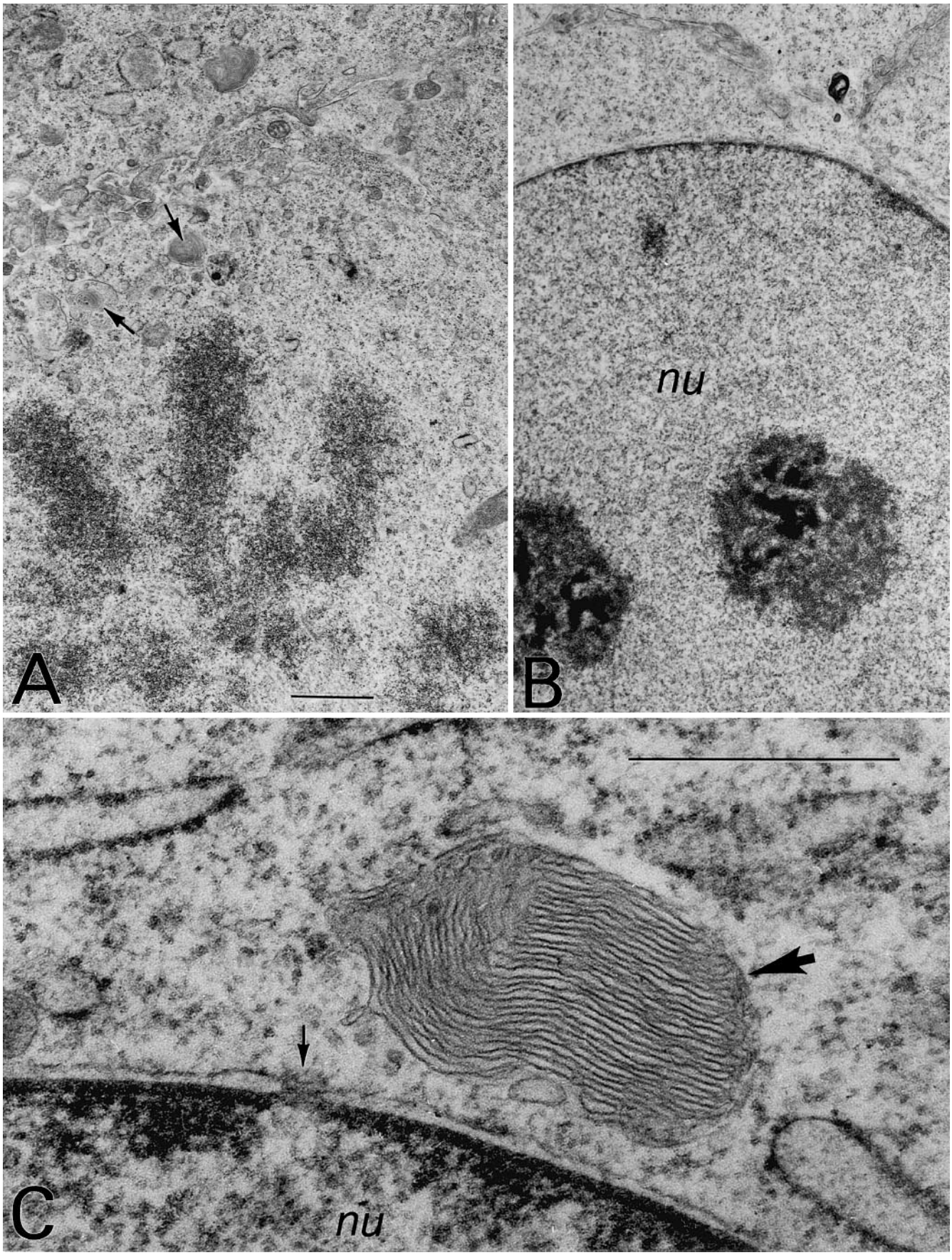
A
B
nu
C
nu

procedure resulted in the development of neurites of longer than 50 μm, which are presumably dendrites [16], and long thin cellular processes resembling axons. Electron microscopic examination (below) of differentiated and undifferentiated cells also identified the consequences of differentiation in a reduced number of nucleoli, the presence of nuclear lobulation, and the characteristics of the cytoplasmic fibrillar network.

Effects of CumOOH on cell viability in differentiated and undifferentiated cells

During the 6-h time course following exposure to CumOOH, a greater percentage of differentiated cells than undifferentiated cells consistently demonstrated trypan blue staining, indicating that differentiation was associated with increased cell mortality (Fig. 1). In both differentiated and undifferentiated cells, loss of viability required the availability of iron; if DETAPAC was added to the media before CumOOH, there was no loss of viability in either differentiated or undifferentiated cells. The protective effect of DETAPAC was expected because scission of CumOOH to the cumene alkoxyl radical and hydroxyl ion requires transition metal catalysis. Addition of CumOOH to a final concentration of 50 μ*M* had no discernible alkalinizing effect on pH in the buffered media, and thus the protective effect of DETAPAC argues that the chemical species responsible in this model system for cell damage and mortality is indeed the cumene alkoxyl radical.

Electron microscopy

Undifferentiated control NB-104 cells

Electron microscopic profiles of undifferentiated NB-104 cells at various stages of mitosis were obtained and characterized. Examples of a dividing cell at metaphase and another cell at interphase are shown in Fig. 2 A and B, respectively. Typically, the nucleus of non-dividing cells contained multiple nucleoli and evenly dispersed heterochromatin (Fig. 2 B). The nuclear envelope was smooth with very few infoldings; small patches of heterochromatin tended to underline its inner aspect, except at regions where nuclear pores were found (Fig. 2 C, small arrow). The cytoplasm of both dividing and nondividing cells contained a rich variety of organelles in an electron-lucent matrix. Among these organelles were elements of the rough endoplasmic reticulum (RER), consisting of short, dilated cisternae studded by ribosomes (Fig. 2 C), clusters of mitochondria, numerous intermediate size filaments, polyribosomes and free ribosomes (Fig. 2 C, 3 A). Whorls of concentrically disposed membranes (Fig. 2 A, arrows) were frequently found in close proximity to the cell membrane, whereas an array of smooth membranous sacs and tubules was occasionally observed in close proximity to the nucleus (Fig. 2 C, large arrow). The cell surfaces were irregular due to the presence of cytoplasmic finger-like processes and bulbous protrusions which resulted from evaginations of the cell membrane (Fig. 3 A, C, small and large arrows). Processes from neighboring cells interdigitated with each other at the free cell borders and within the narrow clefts between closely adjoining borders. Both the processes and the larger protrusions contained smooth membranous sacs, vesicles, polyribosomes and free ribosomes (Fig. 3 C). In addition, a web of microfilaments underlay the cell membrane, and intermediate-size filaments extended from this web into the underlying cytoplasm. Complex vacuoles, consisting of heterogeneous vesicles, dense granules and membranous sacs, appeared to form close to the cell surface (Fig. 3 B); another type of vacuole, consisting primarily of vesicles and tubules, was occasionally observed, seemingly extruding its contents onto the cell surface (Fig. 3 A, upper right corner, and C, arrowhead).

Differentiated control NB-104 cells

After differentiation, the nucleus of most NB-104 cells became lobulated due to extensive infolding of its nuclear envelope (Fig. 4 A, nu). Large patches of condensed heterochromatin were conspicuous throughout the nucleus and at the inner aspect of the nuclear envelope. The cytoplasm of differentiated cells contained RER cisternae, which were branched and somewhat longer than those of undifferentiated cells. Most of the ribosomes between these cisternae and elsewhere in the cytoplasm were in the form of polyribosomes (Fig. 4 A, C). The Golgi apparatus was represented by small complexes consisting of smooth cisternal arrays and their associated vesicles, and was observed primarily in a perinuclear position (Fig. 4 A, C). Numerous alveolate vesicles (Fig. 4 B, arrow) and alveolate residues (Fig. 4 B, arrowheads) were observed close to or at the cell surfaces, indicating a significant shuttling of such vesicles between the Golgi complexes and the cell membrane. Most conspicuous among the organelles was a dense feltwork of interweaving intermediate filaments that pervaded most of the cytoplasm (Fig. 4 C). Many RER cisternae appared to contain these filaments, suggesting their synthesis and assemblage in the RER prior to their translocation to other cytoplasmic sites.

Fig. 3 A–C Profiles of undifferentiated control NB-104 cells. Areas outlined by the *small* and *large rectangles* in **A** are reproduced at higher magnification in **B** and **C**, respectively. **A** Portions of several cells in a cluster, the largest of which contains a portion of the nucleus shown in the *lower left corner*. Intercellular clefts often contain many finger-like processes from neighboring cells. **B** Detail of the cytoplasm of a cell in **A** showing aggregation of vesicles, dense granules and membranous sacs partially surrounded by a membrane *(arrow)*. **C** Detail of the cell surfaces. In addition to finger-like processes *(small arrow)*, bulbous protrusions *(large arrow)* and vesicular vacuoles *(arrowhead)* are found at the cell surface. The indicated bulbous protrusion contains ribosomal arrays, free ribosomes, a mitochondrion *(m)* and vesicles of smooth endoplasmic reticulum. A web of microfilaments underlies the cell membranes and intermediate filaments project from this web into the cytoplasm. *Bars* **A** = 1.0 μm; **B** (also for **C**) = 0.5 μm ▶

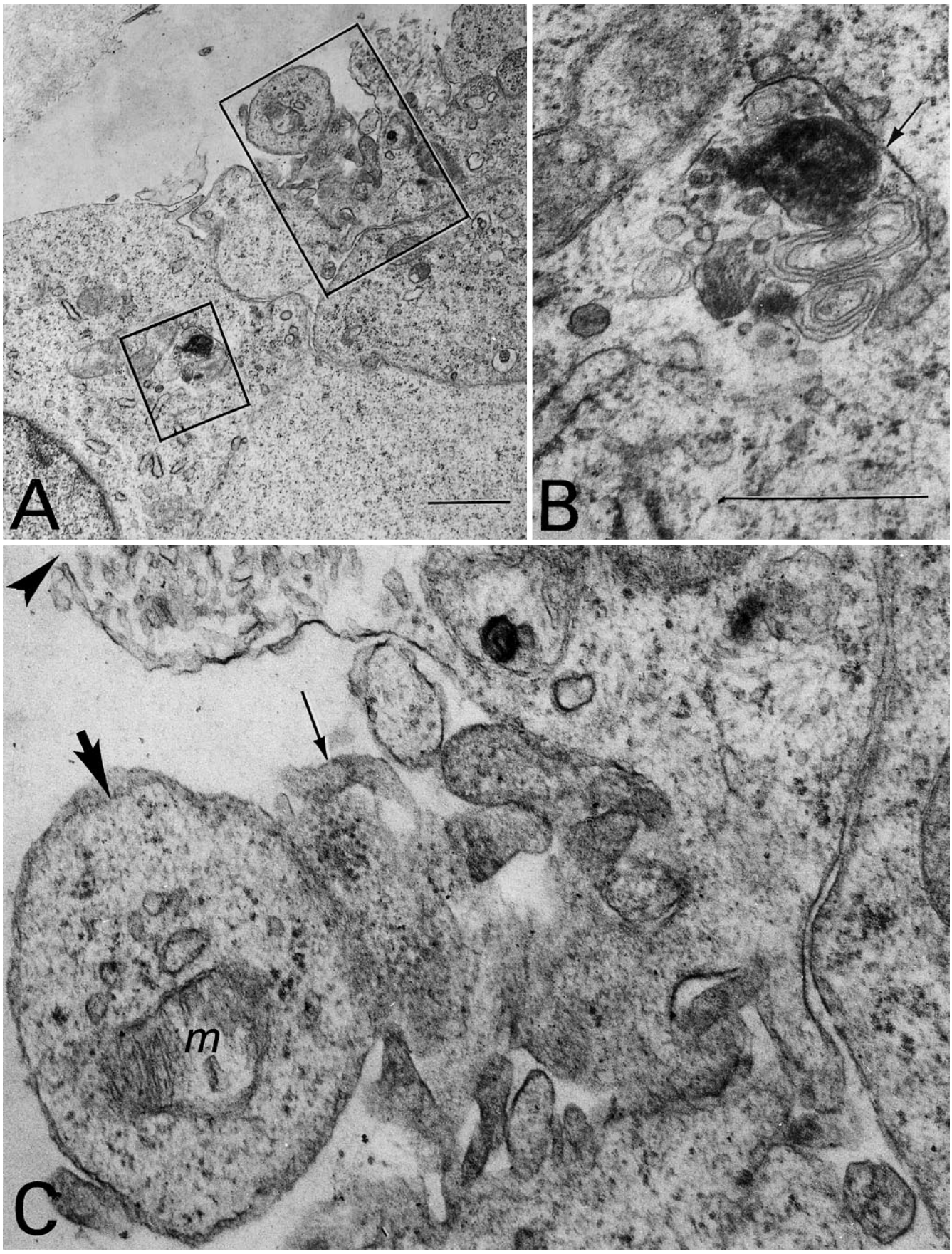
A
B
C
m

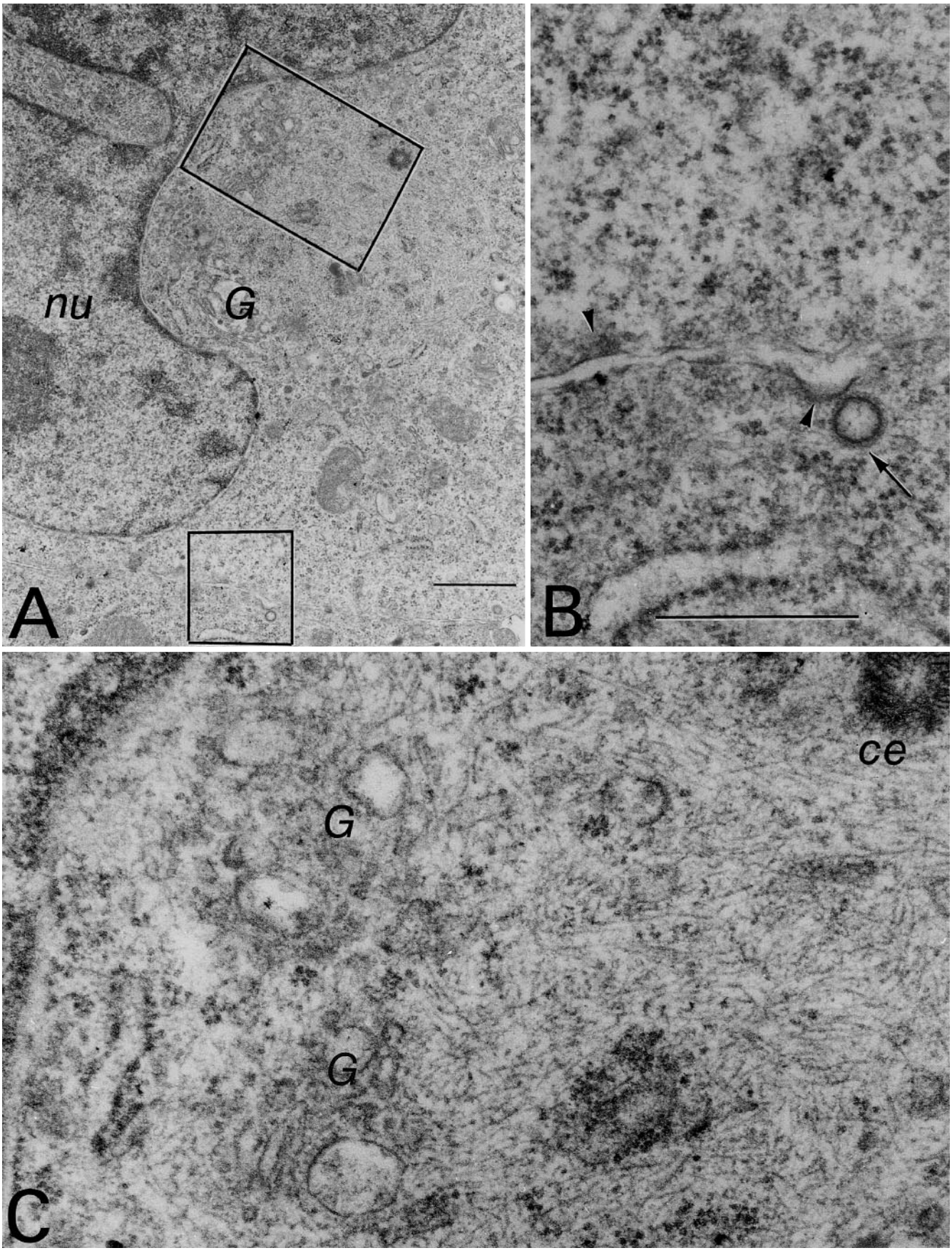
nu
G
A
B
ce
G
G
C

NB-104 cells 2 h after exposure
to cumene-alkoxyl radical

The ultrastructure of undifferentiated NB-104 cells after 2 h of free radical exposure was similar to that of undifferentiated controls. However, at this exposure time the ultrastructure of differentiated cells was affected, with these cells demonstrating moderate to severe alterations of their cytoplasmic organelles. The constituent membranous sacs of the Golgi complexes in moderately affected differentiated cells were fragmented into large vacuoles and vesicles. These cells also displayed numerous abnormal membrane-bound vacuoles in various stages of formation (Fig. 5 A, arrows); some of these vacuoles contained both filament fragments and membranous sacs and tubules (Fig. 5 C). In these cells there was also increased electron density in some of the mitochondria. In spite of these changes, the RER and the polyribosomal arrays throughout the moderately affected differentiated cells remained largely unchanged. In contrast, most organelles of severely affected cells appeared disrupted. In addition to fragmentation of the Golgi complexes, the RER was also fragmented, and many of its associated ribosomes appeared to be fusing with each other (Fig. 5 B, large arrow). Electron-dense bodies, many of which resembled lysosomes, were present. Most of the abnormal vacuoles contained densely packed filament fragments and vesicles, many of which appear to be fusing with the membrane bounding these vacuoles (Fig. 5 B, D, small arrows). Well-organized membranous whorls, similar to those located in the perinuclear region in undamaged cells (Fig. 2 C), were often observed in close proximity to the cell membrane, and in a few cases portions of their outermost membranes were exposed directly to the cell surface (Fig. 5 D, small arrowheads). This last observation suggests that these organelles may have migrated to the cell surface, possibly in an attempt to repair the cell membrane as it became damaged by free radicals (see also Discussion).

NB-104 cells 4 h after exposure
to cumene-alkoxyl radical

After 4 h most undifferentiated NB-104 cells had become moderately affected by the free radical insult (Fig. 6 A, B). As seen for the moderately affected differentiated cells after 2 h, these undifferentiated cells had mostly intact RER and polyribosomes. However, filamentous vacuoles were not present in the cytoplasm. A membranous whorl was occasionally observed at the cell surface, with portions of its outermost membranous layer seemingly attempting to bridge a structural defect (Fig. 6 B, between small arrowheads). In contrast, all differentiated cells showed severe alterations of their ultrastructure after 4 h. As was the case after 2 hours, the most severely damaged organelles were the Golgi complexes (G, Fig. 6 C) and the RER. Vacuolation and microvesiculation of the Golgi membranes were prevalent, as was the presence of abnormal membranous vacuoles and electron-dense mitochondria (Fig. 6 D). It is apparent from these observations that resistance to radical-mediated ultrastructural damage is greater in undifferentiated cells that in differentiated cells.

NB-104 cells 6 h after exposure
to cumene-alkoxyl radical

After 6 h of exposure many undifferentiated cells continued to show only moderate alteration of their ultrastructure, indicating that they were capable of resisting and coping effectively with the damage initiated by the radical. Despite apparent preservation of most RER and polyribosomes, some membrane-bound clusters of discarded ribosomes were observed close to the cell surface (Fig. 7 A, arrow). Other organelles such as mitochondria and intermediate filaments appeared relatively normal (Fig. 7 B). In a fortuitous finding (Fig. 7 C). it became apparent how the cell packages portions of discarded RER. Cisternae of RER which were denuded of their associated ribosomes (Fig. 7 C, small arrow) appeared to coalesce into concentric membranous sacs, which were included into a large vacuole (Fig. 7 C, large arrowhead). Moreover, discarded ribosomes from the denuded RER cisternae (Fig. 7 C, small arrowheads) fused with each other and ap-

◀ **Fig. 4 A–C** Micrographs of a differentiated control NB-104 cell. Areas outlined by the *small* and *large rectangles* in **A** are reproduced at higher magnification in **B** and **C**, respectively. **A** Portion of the nucleus *(nu)* and the cytoplasm of the cell. The nucleus is multilobulated and contains patches of densely aggregated chromatin. The cytoplasm contains small Golgi complexes *(G)*, long cisternae of RER, clustered mitochondria, and numerous ribosomal arrays. **B** Portions of a narrow intercellular cleft flanked by two neighboring cells. Alveolate vesicles *(arrow)* are found in close association with the cleft. Membranes on each side of the cleft often show evidence of vesicular residues suggesting endocytosis or release *(arrowheads)*. **C** Detail of the cytoplasm of the cell in **A** showing small Golgi complexes *(G)*, ribosomal arrays, and a dense feltwork of intermediate filaments. A centriole *(ce)* is seen in the *upper right corner*. *Bars* **A** = 1.0 μm, **B** (also for **C**) = 0.1 μm

Fig. 5 A–D Examples of differentiated NB-104 cells exposed to ▶ free radical insult for 2 h. Areas outlined by *rectangles* in **A** and **B** are reproduced at higher magnifications in **C** and **D**, respectively. **A** An example of a moderately affected cell containing a nucleus *(nu)* surrounded by an irregularly contoured envelope. Although vacuolation an vesiculation of the Golgi complex *(G)* as well as increased electron density of some mitochondria are noticeable, other organelles such as the RER and ribosomal arrays appear less affected. Large vacuoles *(arrows)* containing membranous tubules and sacs are also observed. **B** Most of the micrograph is occupied by a portion of a cell with severe alterations of its organelles. Vacuoles with vesicles and filaments *(arrows)* in various stages of formation are observed, as well as RER in a state of fragmentation *(large arrow)*. **C** A membranous vacuole containing an array of membranous tubules sectioned in different planes. **D** A membranous vacoule containing densely packed material of a filamentous or granular nature. Also contained in this vacoule are membranous vesicles, some of which appear to fuse with the membrane of the vacuole *(small arrows)*. A *large arrow* points at a membranous 'whorly' body with portions of its outermost membranes exposed to the cell surface. *Bars* **A** (also for **B**) = 1.0 μm, **C** (also for **D**) = 0.1 μm

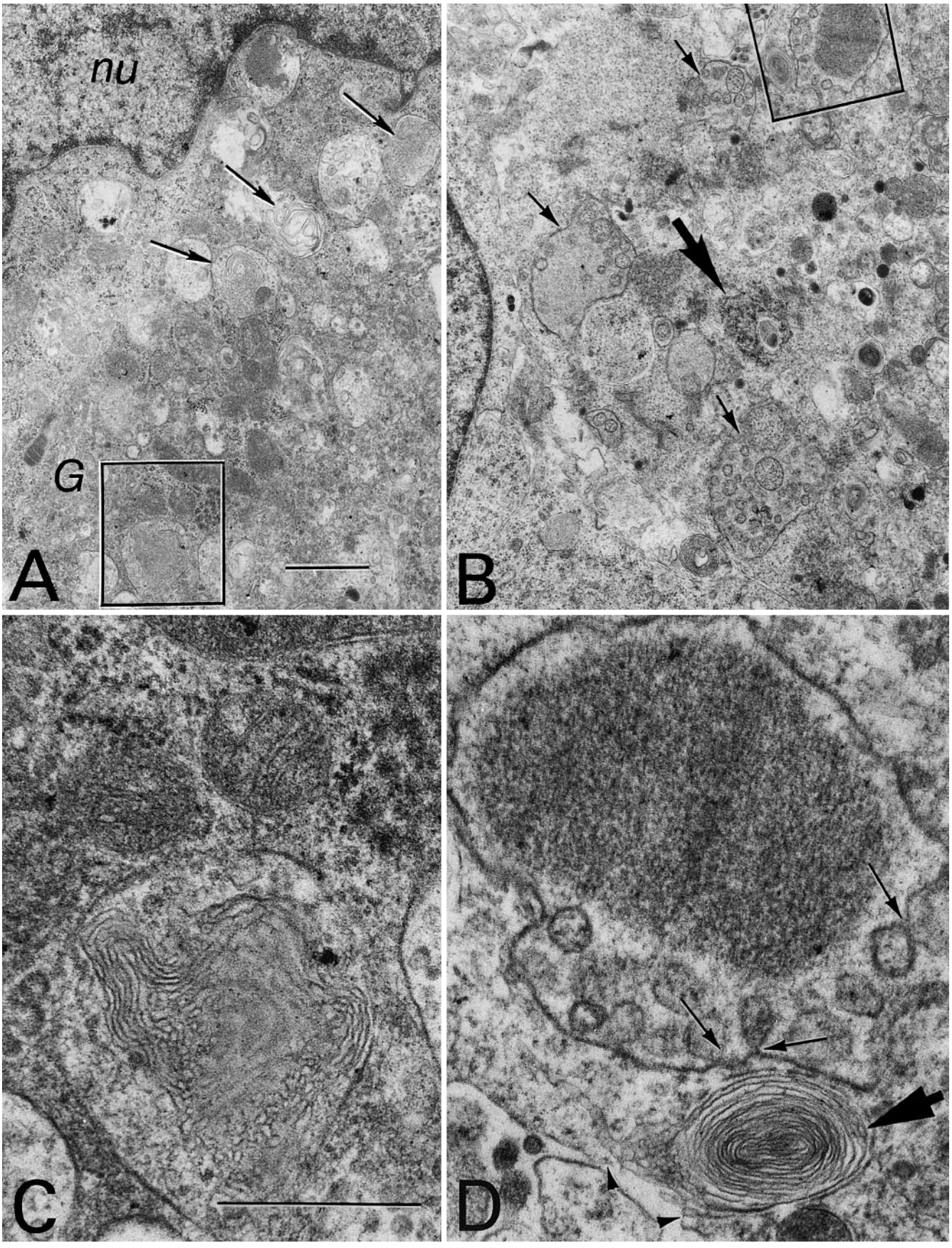

Fig. 5A–D

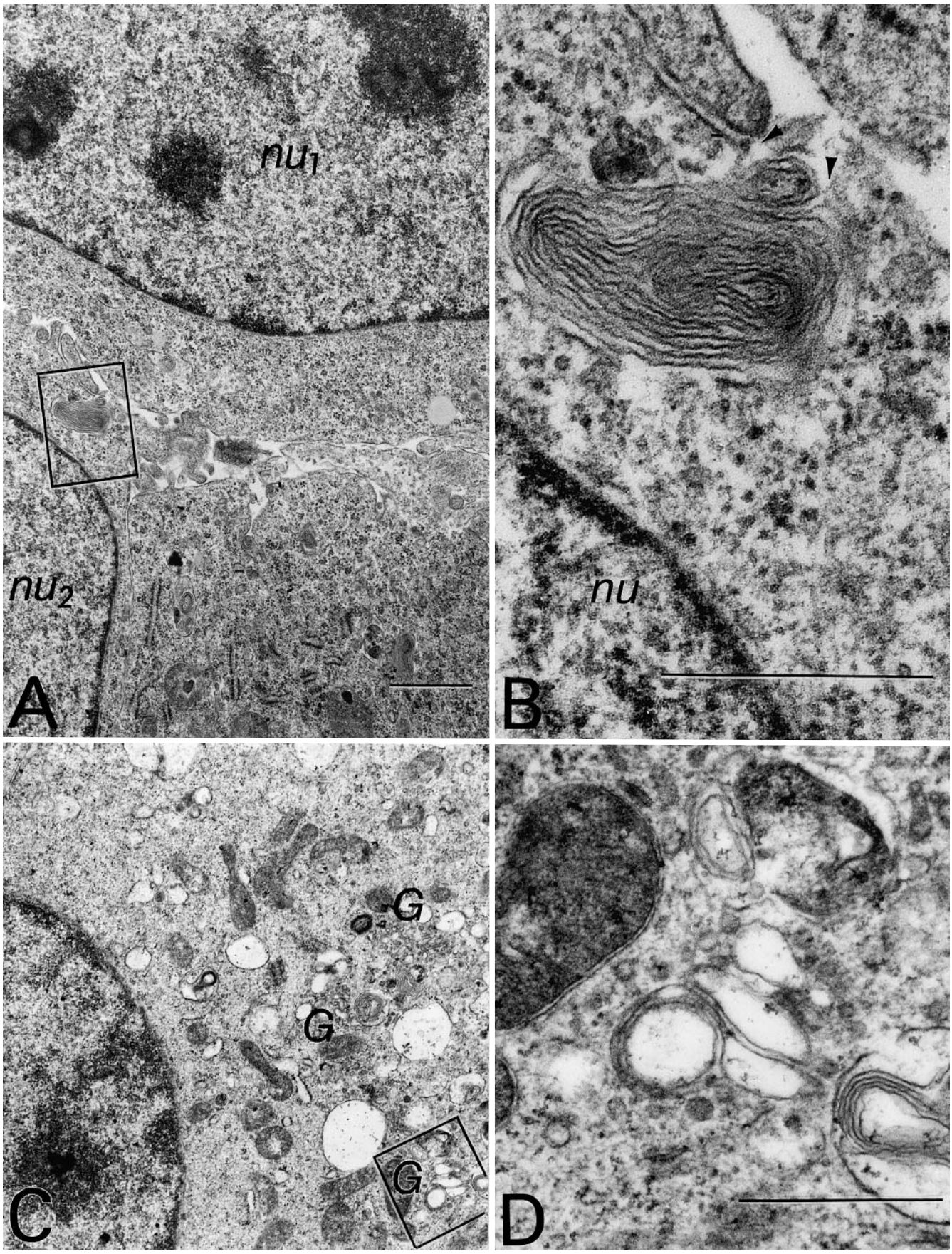

Fig. 6 A–D (for legend see next page)

peared in the process of being enclosed into another vacuole (Fig. 7 C, large arrow), similar to that shown in Fig. 7 A (arrow). While the fate of these heterogeneous vacuoles with RER debris is uncertain, both of these types of vacuoles were found close to the cell surface (Fig. 7 A, 8), suggesting that their contents were destined for exocystosis.

In contrast to the undifferentiated cells, the majority of differentiated cells after 6 h of exposure showed severe alterations of the nucleus and cytoplasm. The nucleus became smaller and had a rough envelope due to many infoldings. It also contained large patches of heterochromatin, in some cases forming a bull's eye configuration similar to that found in early pyknotic nuclei (Fig. 9 A, nu1, nu2) at the light level. The cytoplasm was electron dense due to close packing of organelles in a shrunken cytoplasm. The ultrastructure of most organelles was severely compromised, and cytoplasmic debris was found at the cell surfaces and between neighboring cells (Fig. 9). At high magnification, long stretches of the plasmalemma appeared fragmented (Fig. 9 B, arrowheads). This observation suggests that cytoplasmic extrusion ultimately leads to the apparent loss of cell volume.

Discussion

Effects of differentiation

The neuronal differentiation that we induced in the NB-104 cells had several effects at the ultrastructural level. In undifferentiated cells we consistently observed multiple nucleoli and dispersed heterochromatin, and several of these cells were actively engaged in mitosis (Fig. 2). Differentiated cells were characterized by single nucleoli, a more condensed heterochromatin pattern, greater complexity and organization of both Golgi and RER, enhanced numbers of ribosomal rosettes, a substantial increase in cytoskeletal intermediate filaments, and an increased population of alveolate vesicles that are involved in receptor-mediated endocytosis and traffic between the plasmalemma and Golgi (Fig. 4) [12]. In general, these observations are consistent with there being an overall increase in order, complexity, and protein synthesis in association with differentiation; these observations are also consistent with previous studies of the structural characteristics induced by neuronal differentiation [10, 16, 25].

Chemistry of damage initiation by CumOOH

The ultrastructural damage induced by the initial exposure of the cells to CumOOH in media containing 3 μ*M* iron was progressive over the time course we examined. This is unlikely to be due to ongoing reactions involving the cumene moiety itself. The iron in the media must be principally ferrous because ferric iron salts have solubility constants on the order of 10^{-18}, and readily visible ferric iron precipitates are formed from even micromolar solutions. The homeolytic cleavage by ferrous iron of hydroperoxides to generate oxyl radicals and hydroxyl ion is stochiometric, rapid, and able to progress through redox recycling of the metal. In addition, reactions involving electron abstraction by oxyl radical species also proceed rapidly [2]. Thus we utilized a reaction system that involved rapid scission of CumOOH followed by rapid reduction of the cumene alkoxyl radical to generate the stable cumene alcohol moiety. Both cholesterol and unsaturated fatty acids in membranes undergo rapid oxidation by alkoxyl radicals and then engage in the exponentially propagating reactions of lipid peroxidation [2]. Thus, in the system utilized here, the initial damage most likely involves inititation of lipid peroxidation at the plasmalemma, and the progressive cellular mortality and ultrastructural damage reflects the consequences of the propagating radical reactions, as directly demonstracted in other investigations [24].

Effects of differentiation on cell susceptibility to radical damage

Differentiated cells were more susceptible than undifferentiated cells to radical-induced damage along the time course of this study. In undifferentiated cells we did not observe substantial evidence of ultrastructural damage until 4 h after the initial exposure to CumOOH. In contrast, differentiated cells showed evidence of damage at all times studied. Our observation that differentiated cells are

◀ **Fig. 6** Profiles of undifferentiated (**A, B**) and differentiated (**C, D**) NB-104 cells exposed to free radical insult for 4 h. Areas outlined by *rectangles* in **A** and **C** are reproduced at higher magnification in **B** and **D**, respectively. **A** Cluster of cells two of which show portions of their nuclei *(nu_1, nu_2)*. All the cells in the cluster are moderately affected by the free radical insult. **B** A membranous 'whorly' body adjacent to the intercellular cleft. Note that the outermost membranes appear to extend into a gap *(between arrowheads)* at the cell membrane. **C** Portion of a cell with severe alteration of the Golgi complexes *(G)*, RER, and other cytoplasmic organelles. **D** Detail of a Golgi complex showing vesiculation and vacuolation of its membranous sacs. Note the electron density of the adjacent mitochondrion. *Bars* **A** (also for **C**) = 1.0 μ, **B** = 0.5 μm, **D** = 0.1 μm

Fig. 7 A–C Micrographs of undifferentiated NB-104 cells exposed to free radical insult for 6 h. Area outlined by the *rectangle* in **A** is reproduced at higher magnification in **B**. **A** Portion of a cell cytoplasm close to the cell surface. Most organelles are intact. Vacuoles primarily contain discarded ribosomes *(arrow)* or smooth membranous sacs *(arrowhead)*. **B** Detail of a mitochondrion. Note the integrity of the inner cristae particles and the presence of an electron dense granule *(arrow)*. **C** This micorgraph illustrates the putative formation of different types of vacuoles after free radical insult. The *left half* shows sacs of RER, many of which have lost their associated ribosomes *(small arrowheads)*. Many of the ribosomes in the *center* of the array have coalesced and appear to be enclosed into a vacuole similar to that shown in **A** *(arrow)*. On the *right side* of the figure another vacuole *(large arrowhead)* appears to originate also from the RER *(arrow)*. *Bars* **A** 1.0 μm, **B** (also for **C**) = 0–1 μm ▶

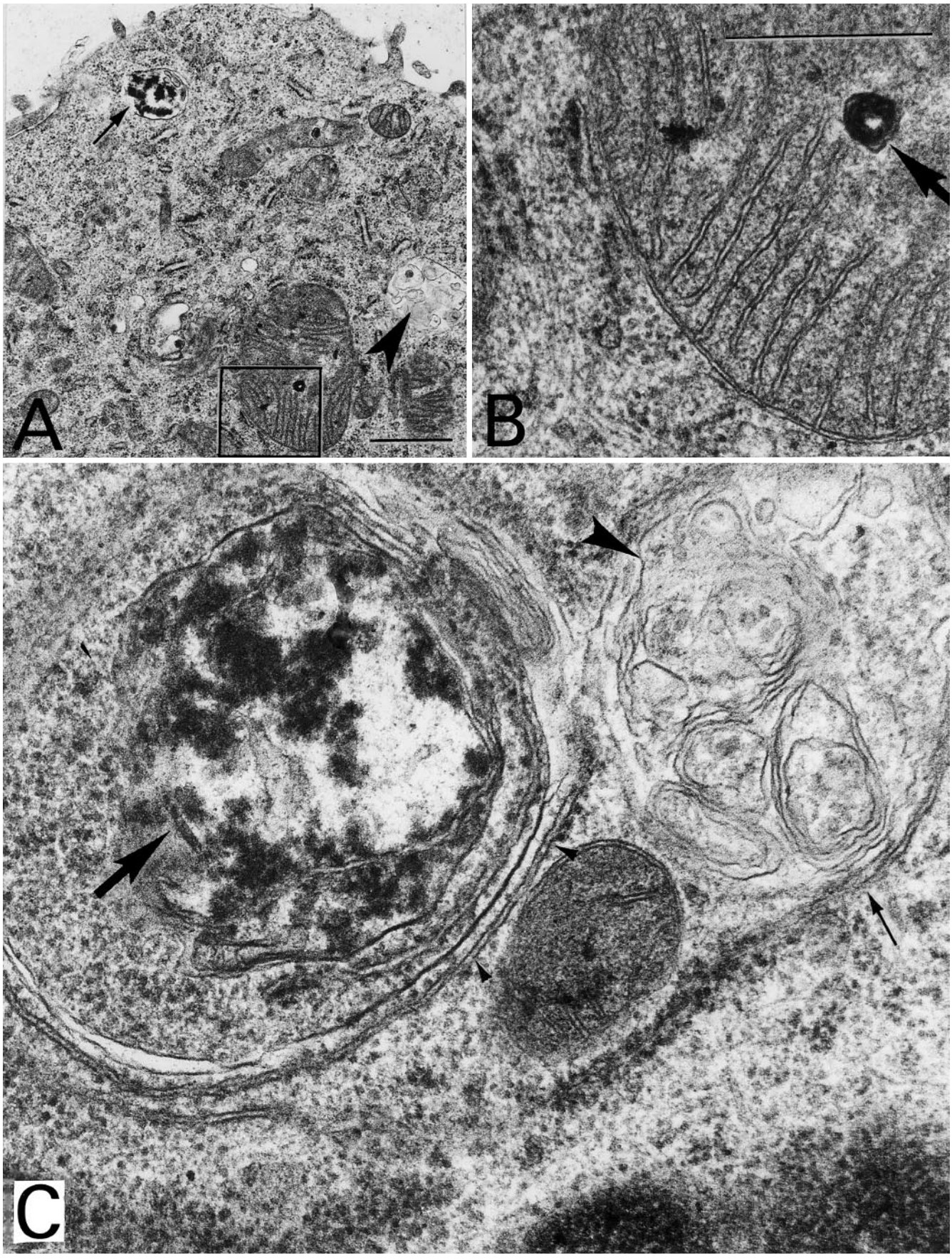
A
B
C

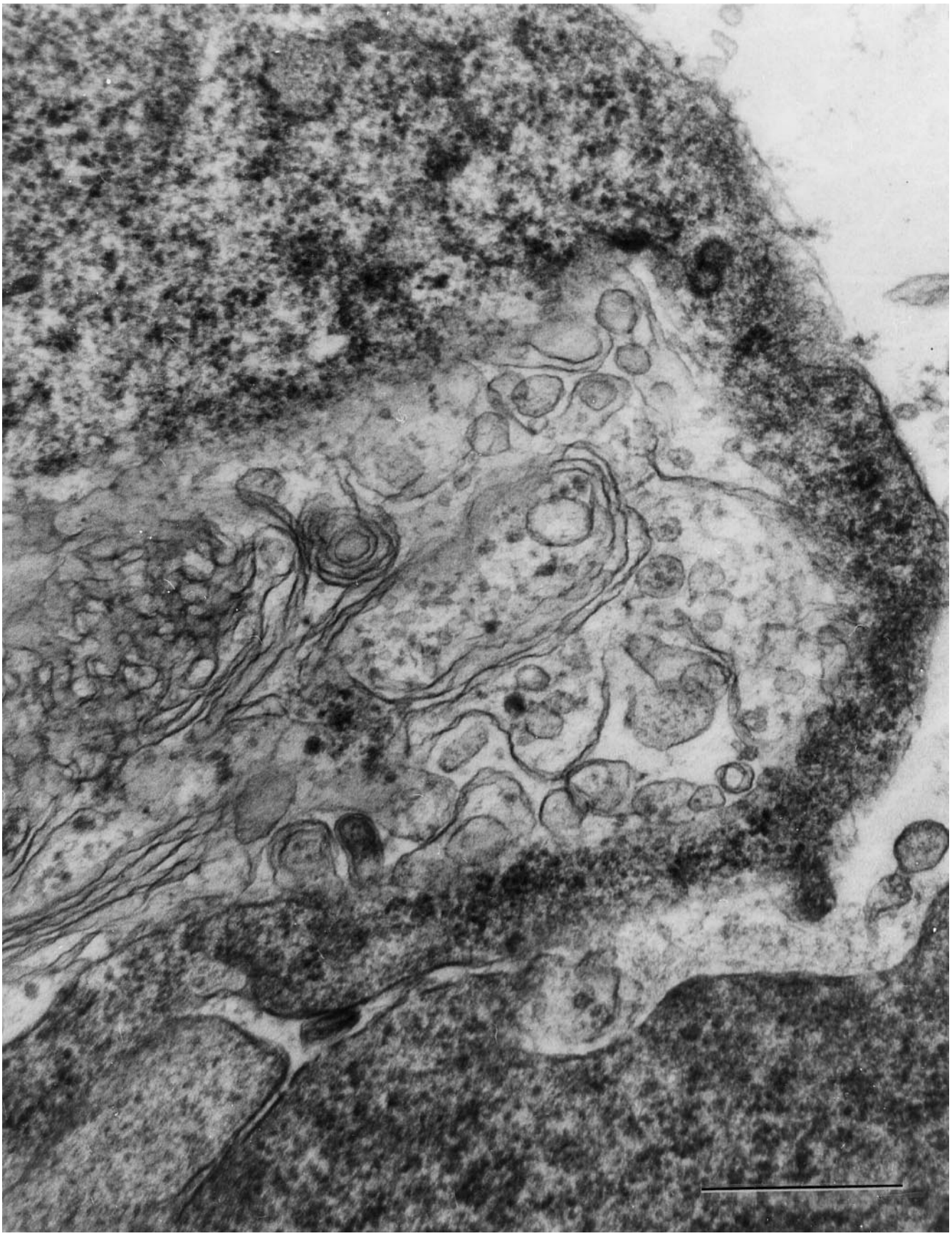

Fig. 8 Portion of undifferentiated NB-104 cell exposed to 6 h of free radical insult. A large vacuole containing randomly organized smooth membranous sacs and vesicles is located close to the cell surface. This complex organelle is morphologically different than the membranous 'whorly' body shown in previous micrographs, and most likely includes material destined for exocytosis. *Bar* = 0.1 μm

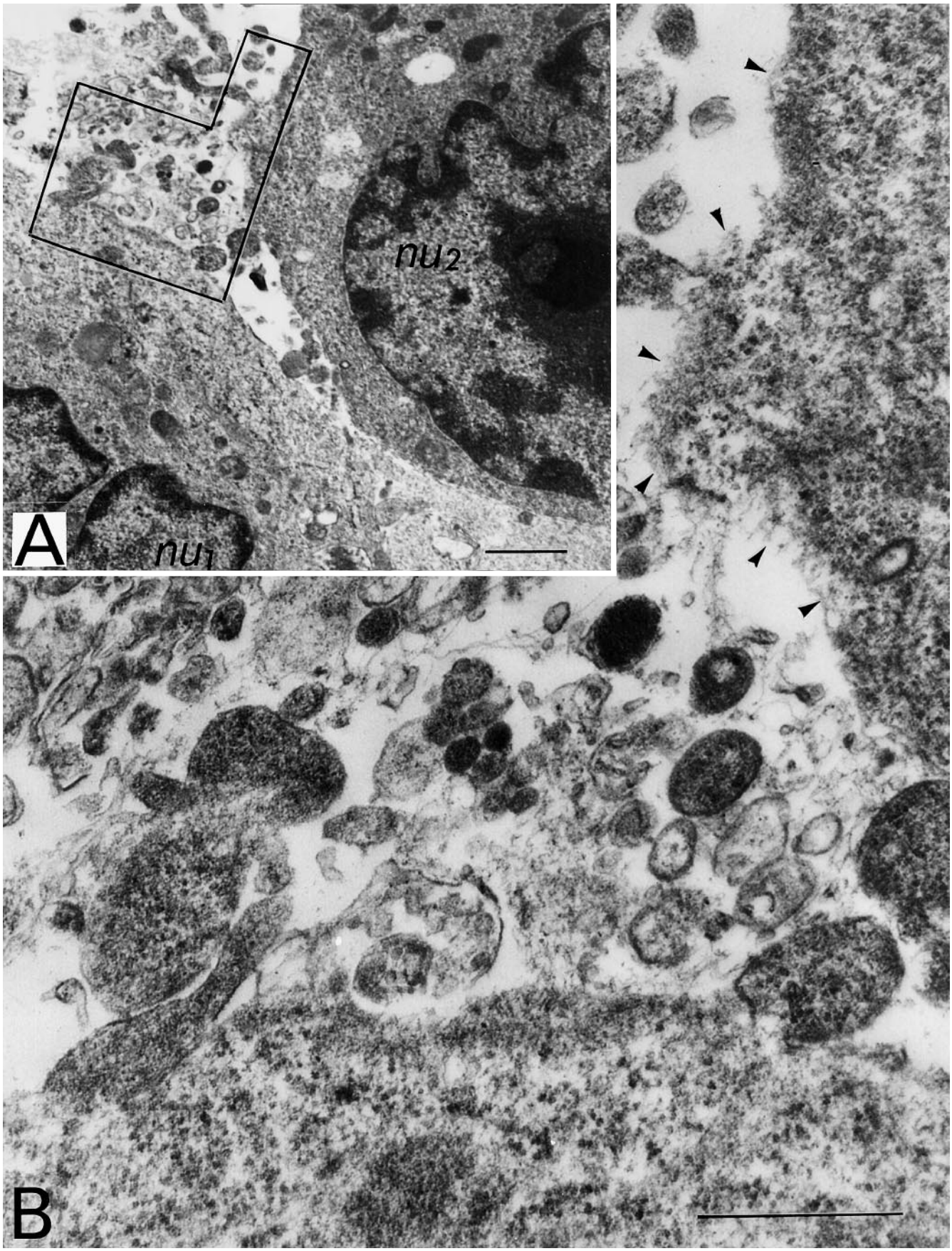

Fig. 9 A, B Profiles of NB-104 differentiated cells exposed to 6 h of free radical insult. Enclosed area in **A** is reproduced at a higher magnification in **B**. **A** Portions of two cells containing shrunken nuclei *(nu_1, nu_2)* with densely aggreagated chromatin reminiscent of the early stages of apoptosis. The cyoplasm of both cells is very electron dense due to the condensation of organelles, probably due to shrinkage. **B** Cytoplasmic organelles and other cellular debris are found in large numbers outside of the cells and close to their surfaces. The cell membranes appear fragmented *(arrowheads)*, thus increasing the probability of organelle extrusion. *Bars* **A** = 1.0 μm, **B** = 0–1 μm

more sensitive to radical damage is consistent with previous reports [6]. This evidence indicates that neuronal differentiation is associated with metabolic alterations that have substantial implications for the cell's capacity to manage radical damage originating in the plasmalemma. Two specific alterations associated with differentiation that may diminish resistance to radical damage in the affected membranes are down-regulation of lipid and sterol synthesis [5, 21] and reduction of the AP-1 transcription promoter binding complex comprised of heterodimers formed between c-FOS and c-JUN [1]. Radical damage caused by ionizing radiation induces c-fos and c-jun transcripts [7], and the family of genes with AP-1 consensus sequences in their promoters include several genes encoding proteins important in defense against electrophiles [17, 18], e.g., glutathione transferase, NADP(H) quinone reductase, epoxide hydrolase, and UDP glucuronyl transferase. It is interesting to note that phenobarbital induces expression of this electrophile defense group through radical-mediated mechanisms [15]. One would also expect enhanced activity of this electrophile defense group during DNA replication because of the crucial involvement of the AP-1 complex in the cell cycle [1]. Enhanced radical defense during cell division could prevent replication errors that would be associated with electrophilic damage to DNA at this critical time. These considerations suggest that the resistance to radical-induced membrane damage in undifferentiated cells potentially involves enhancement of defense against electrophilic attack as well as up-regulation of the capacity for lipid synthesis and membrane repair.

Organelle differential susceptibility

We observed substantial differences in the sensitivity of various organelles to radical-mediated damage. The nuclear envelope and mitochondria retained ultrastructural integrity throughout the time course examined, but in differentiated cells early damage was observed in the plasmalemma, Golgi, and RER. After longer reaction times, similar damage was observed in undifferentiated cells.

This subcellular pattern of damage has several implications. First, the relative resistance of the mitochondria and nuclei to radical-induced ultrastructural damage is consistent with our previous reports that global brain ischemia and reperfusion are not associated with radical damage to nuclear [27] or mitochondrial [28] DNA. In the present study both the nuclear envelope and the mitochondrial membrane demonstrate substantially greater resistance to damage by radical mechanisms than the membranes of the plasmalemma, Golgi, and RER. Higuchi and Linn [8] have recently reported that H_2O_2-induced lethal injury to HeLa cells need not involve either radical-mediated fragmentation of mitochondrial DNA nor a significant increase in 8-OH-deoxyguanosine. Taken together, these results indicate that damage to specific membrane systems is more fundamental than DNA damage in early cell death induced by radicals.

The ultrastructural alterations in the plasmalemma, Golgi, and RER induced by radical mechanisms in this study are similar in morphology and time course to the ultrastructural consequences observed in SVNs during reperfusion following global brain ischemia [11, 14, 19]. This and the histochemical evidence for lipid peroxidation products in these neurons within the first 90 min of reperfusion [30] support the inference that radical mechanisms are responsible for the ultrastructural modifications observed in SVN plasmalemma, Golgi, and RER during the first few hours of post-ischemic brain reperfusion.

Alterations in vesicular trafficking and vacuoles

Our experiments reveal that radical damage induces a prominent alteration in the ultrastructure and trafficking of vesicles and vacuoles. We frequently observed a well-organized membrane whorl that did not appear to have other contents and was located near the nucleus in undifferentiated cells prior to damage (Fig. 2). After radical damage this structure appeared to have been transported to the plasmalemma (Fig. 5 D, 6 B) and be involved in "patching" early damage in both undifferentiated and differentiated cells. The appearance of this process is consistent with the recent observation that resealing of the plasmalemma occurs by a vesicular mechanism [23]. Radical damage also induced the accumulation of numerous small vacuoles in the area of the Golgi (Fig. 6 C, D). These vacuoles appeared to undergo coalescence into larger poorly organized multi-layered membranous vacuoles that contained filament fragments and were ultimately extruded from the cell. Indeed, these vacuoles appear to be formed for the purpose of mobilization and ultimate extrusion of degraded organelle components; Fig. 7 C shows two adjacent vacuoles, one containing primarily ribosomal debris and the other the membranous sacks that are formed by vesicular fusion. These vacuoles can be seen either very close to the cell surface or being ejected from the cell (e.g. Fig. 8). This suggests a general injury management mechanism in which damaged organelle components are selectively packaged and extruded from the cell.

Other investigators have observed similar cytoplasmic bodies containing poorly organized concentric vesicles that are induced under differing circumstances. Whorls containing RER in adrenal stem cells are transformed into whorls of smooth ER by adrenocorticotropic hormone stimulation and are probably involved in secretion by these cells [13]. Abnormal concentric cytoplasmic bodies are seen in Tay-Sachs neurodegeneration [20], which involves the pathological accumulation of ganglioside lipids, and in the Gunna Rat model of Crigler-Najar syndrome [3], a neurogenerative disorder associated with glucuronyl transferase deficiency. Hwang et al. [9] observed that cyclohexamide, but not puromycin, caused formation of poorly organized whorly stuctures containing other organelles in rat liver. Cyclohexamide interferes with protein synthesis by polyribosomes on the RER, and treatment with this agent was associated with inhibition of leucine

incorporation accompanied by an increase in choline incorporation before the appearance of the whorly structures. This led these investigators to postulate [9] that, in this system, formation of the membrane whorls was linked to desynchronization of the synthesis of the protein and lipid components required for normal formation or repair of membranes. The ultrastructural appearance of these poorly organized concentric cytoplasmic bodies is very similar to those observed both in the present study and in previous studies of the ultrastructural consequences of brain reperfusion [14, 19]. Taken together, these observations suggest that formation of the abnormal concentric vacuoles in the area of the Golgi is associated with abnormal lipid metabolism and membrane recycling, and in our study this was induced by radical damage. Thus, we believe that during post-ischemic brain reperfusion these ultrastructural alterations are induced by radical mechanisms whose reaction products can in fact be observed in SVNs [30].

Acknowledgements This study was supported in part by PHS-NIH-NINDS grant NS01585 and by the Emergency Medicine Foundation-Genetech Center for Excellence Award. We are grateful for the use of the JEOL-JEM 1010 electron microscope in the Detroit Neurotrauma Center.

References

1. Angel P, Karin M (1991) The role of Jun, Fos and the AP-1 complex in cell-proliferation and transformation. Biochim Biophys Acta 1072:129–157
2. Aust SD, White BC (1986) The role of iron in lipid peroxidation. In: Rice-Evans C (ed) Free radicals, cell damage, and disease. Richelieu Press, London, pp 15–27
3. Batty HK, Millhouse OE (1976) Ultrastructure of the Gunn rat substantia nigra. I. cytoplasmic changes. Acta Neuropathol (Berl) 35:93–107
4. Bottenstein JE, Sato GH (1979) Growth of a neuroblastoma cell line in serum-free media. Proc Natl Acad Sci USA 76:514–517
5. Cooper RA, Ip SHC, Cassileth PA, Kuo AL (1981) Inhibition of sterol and phospholipid synthesis in HL-60 promyelocytic leukemia cells by inducers of myeloid differentiation. Cancer Res 41:1847–1852
6. Dianzani MU (1989) Lipid peroxidation and cancer: a critial reconsideration. Tumori 75:351–357
7. Higo H, Lee JY, Satow Y, Higo K (1989) Elevated expression of proto-oncogenes accompany enhanced induction of heat-shock genes after exposure of a rat embryos in utero to ionizing radiation. Teratogenesis Carcinog Mutagen 9:191–198
8. Higuchi Y, Linn S (1995) Purification of all forms of HeLa cell mitochondrial DNA and assessment of damage to it caused by hydrogen peroxide treatment of mitochondria or cells. J Biol Chem 270:7950–7956
9. Hwang KM, Yang LC, Carrico CK, Schulz RA, Schenkman B, Sartorelli AC (1974) Production of membrane whorls in rat liver by some inhibitors of protein synthesis. J Cell Biol 62:20–31
10. Kubo Y (1989) Development of ion channels and neurofilaments during neuronal differentiation of mouse embryonal carcinoma cell lines. J Physiol 409:497–523
11. Kumar K, Goosman M, Krause GS, White BC (1987) Ultrastructural and ionic changes in global ischemic dog brain. Acta Neuropathol (Berl) 73:393–399
12. Lamaze C, Schmid SI (1995) The emergence of clathrin-independent pinocytic pathways. Curr Opin Cell Biol 7:573–580
13. Nickerson PA (1977) Formation of concentric whorls of rough endoplasmic reticulum in the adrenal gland of the mongolian gerbil. J Anat 124:383–391
14. Petito CK, Pulsinelli A (1984) Sequential development of reversible and irreversible neuronal damage following cerebral ischemia. J Neuropathol Exp Neurol 43:141–153
15. Pinkus R, Bergelson S, Daniel V (1993) Phenobarbital induction of AP-1 binding activity mediates activation of glutathione S-transferase and quinone reductase gene expression. Biochem J 290:637–640
16. Prasad KN (1975) Differentiation of neuroblastoma cells in culture. Biol Rev 50:129–265
17. Prestera T, Holtzclaw WD, Zhang Y, Talalay P (1993) Chemical and molecular regulation of enzymes that detoxify carcinogens. Proc Natl Acad Sci USA 90:2965–2969
18. Prestera T, Zhang Y, Spencer SR, Wilczak CA, Talalay P (1993) The electrophile counterattack response: protection against neoplasia and toxicity. Adv Enzyme Regul 33:281–296
19. Rafols JA, O'Neil BJ, Krause GS, Neumar RW, White BC (1995) Global brain ischemia and reperfusion: Golgi apparatus ultrastructure in neurons selectivity vulnerable to death. Acta Neuropathol 90:17–30
20. Samuels S, Gonatas NK, Weiss M (1965) Formation of the membranous cytoplasmic bodies in Tay-Sachs disease: an in vitro study. J Neuropathol Exp Neurol 24:256–264
21. Siperstein MD (1984) Role of cholesterogenesis and isoprenoid synthesis in DNA replication and cell growth. J Lipid Res 25:1462–1468
22. Shubert D, Heinemann S, Carlisle W, Tarikas H, Kimes B, Patrick J, Steinbach JH, Culp W, Brandt BL (1974) Clonal cell lines from the rat central nervous system. Nature 249:224–227
23. Steinhardt RA, Bi G, Alderton JM (1994) Cell membrane resealing by a vesicular mechanism similar to neurotransmitter release. Science 263:390–393
24. Takemura G, Onodera T, Ashraf M (1994) Characterization of exogenous hydroxyl radical effects on myocardial function, metabolism, and ultrastructure. J Mol Cel Cardiol 26:441–454
25. Takemura R, Okabe S, Kobayashi N, Hirokawa N (1993) Reorganization of brain spectrin during differentiation of PC12 cells. Neuroscience 52:381–391
26. Tiffany BR, White BC, Krause GS (1995) Nuclear-envelope nucleoside triophosphatase kinetics and mRNA transport following brain ischemia and reperfusion. Ann Emerg Med 25:809–817
27. White BC, DeGarcia DJ, Krause GS, Skjaerlund JM, O'Neil BJ, Grossman LI (1991) Brain nuclear DNA survives cardiac arrest and reperfusion. J Free Rad Biol Med 10:125–135
28. White BC, Tribhuwan RC, Vander Laan DJ, DeGarcia DJ, Krause GS, Grossman LI (1992) Brain mitochondrial DNA is not damaged by prolonged cardiac arrest or reperfusion. J Neurochem 58:1716–1722
29. White BC, Grossman LI, Krause GS (1993) Membrane damage and repair in brain injury by ischemia and reperfusion. Neurology 43:1656–1665
30. White BC, Daya A, DeGarcia DJ, O'Neil BJ, Skjaerlund JM, Krause GS, Rafols JA (1993) Fluorescent histochemical localization of lipid peroxidation during brain reperfusion following cardiac arrest. Acta Neuropathol 86:1–9